Paper V

SCA2003-08: COMPLEMENTARY IMAGING TECHNIQUES APPLYING NTI AND MRI DETERMINED WETTABILITY EFFECTS ON OIL RECOVERY MECHANISMS IN FRACTURED RESERVOIRS

Graue[1], A., Baldwin[2], B.A., Aspenes[1], E., Stevens[3], J.,Tobola[3], D.P., Zornes[3], D.R.
[1] University of Bergen, Norway, [2] Green Country Petrophysics, Dewey, Oklahoma, USA,
[3] ConocoPhillips, Bartlesville Technology Center, Bartlesville, Oklahoma, USA.

ABSTRACT

The effects of fractures on oil recovery and *in-situ* saturation development in fractured chalk blocks have been determined for several representative wettabilities. These effects were visualized using two complimentary two-dimensional *in-situ* imaging techniques; nuclear tracer imaging (NTI) for the experiments with large blocks of chalk and magnetic resonance imaging (MRI) for high spatial resolution to visualize fluid flow patterns inside fractures between two stacked core plugs. For three different wettabilities, the specific patterns of saturation development were monitored with NTI and the mechanisms of fracture crossing were determined using MRI.

INTRODUCTION

Although oil is produced in huge volumes each day, the expulsion, transport and oil left in the reservoir are determined at the microscopic level. Both the rate and ultimate production are strongly affected by the interaction between the mobile oil and the immobile surface, commonly referred to as wettability, and the shape of the porous network through which the oil and the water flow. These parameters reflect a range of nanometers to hundreds of micrometers [1]. To accurately and reliably simulate and predict reservoir production, the numerical models used must be based on the actual production mechanisms. Therefore, experimental determinations, using representative physical models, are needed to determine production mechanisms and their dependency on reservoir variables such as wettability, pressure differential, fracture size, etc.

The oil recovery mechanisms involved with waterflooding fractured chalk blocks were found to be critically dependent on the wettability of the chalk and contact between adjacent blocks [2-8]. At strongly water-wet conditions, water flow stopped at each fracture until the imbibition endpoint was reached in the preceding matrix block. Then water moved into the next matrix block expelling the oil on a block-by-block basis. At moderately water-wet conditions, water moved across the fractures almost as if they were not there, expelling the oil as if the individual blocks were one continuous block.

In this paper we will present additional work, which shows the impact of changing the flow rate, fracture width and an even lower wettability than previously reported.

EXPERIMENTAL

Rock and Fluids. Preparation of the Rørdal outcrop chalk blocks, for large-scale experiments, has been reported previously [2-4]. The description of the fluids and large blocks used in this study are summarized in Tables 1 and 2, respectively. For the small-scale experiments, three 1½-inch core plugs were drilled from Rørdal outcrop chalk. The core plugs were dried at 60°C for 3 days, vacuum evacuated to 10 mBar and saturated with degassed brine. Porosity was determined by weight and absolute permeability to brine was measured using a biaxial core holder. A summary of the core plug data is given in Table 3 for three wettabilities.

Initial Water Saturations and Wettability Conditions. The strongly water-wet blocks were oilflooded to S_{wi} of 22-28%PV using decane, with a maximum differential pressure of 125kPa/cm. The moderately water-wet blocks were flooded with North Sea stock tank crude oil and were carried out at 90°C in a heated pressure vessel. Blocks were aged to the desired wettability with crude oil at 90° C using a previously published procedure [2-5]. Wettability was determined by the Amott-Harvey method [9] with I_w, the water index, 0.9-1.0 for strongly water-wet, 0.5-0.8 for moderately water-wet and 0.0-0.4 for nearly neutral-wet.

Fracture preparation. The larger chalk blocks were cut into individual smaller blocks, at S_{wi}, and reassembled into the orientation shown in Fig. 1b. The blocks were cut with a band saw and reassembled to produce "closed" and open fractures. The "closed" fractures were assembled with the matrix touching and a small axial force applied during assembly to provide at least some capillary continuity. The open fracture, at 13 cm, was held at 2mm, with a Teflon® spacer. During waterflooding the blocks were positioned vertically such that gravity was aligned with the open fracture.

For the stacked plug experiments each original core plug was cut, after aging, into two plugs and the fracture located at the cut, to ensure a continuous wettability distribution across the fracture. The two half plugs were stacked horizontally, separated by a fracture that was varied from 1-3.5 mm using Teflon® spacers. Shrink tube held the cores and spacer(s) in place and an applied confinement pressure prevented bypass. The assembled set of two core plugs is shown in Figure 2, with a representative MRI image taken across the fracture.

Saturation monitoring. Nuclear-tracer imaging (NTI) was used to monitor waterflooding of the chalk blocks, first whole, then fractured. Two-dimensional brine saturations were determined by measuring gamma ray emission from either ^{22}Na or ^{60}Co dissolved in the brine at each point of the grid shown in Figure 1a. The principles and application of the NTI technique have been described in detail previously [10-13].

The *in-situ* fluid saturation distribution for the stacked core plug/fracture system was monitored with magnetic resonance imaging (MRI) [1,14-16]. To distinguish between water and decane, the water was replaced with deuterium oxide, D_2O, in a miscible displacement at residual oil saturation. Thus, only the decane was imaged. The transport mechanism for the wetting phase into and across the fracture was determined for each

experiment, with the variables being wettability, flow rate and fracture aperture. The average saturation of water and decane were confirmed with low-field NMR (Nuclear Magnetic Resonance) spectroscopy, to check the efficiency of the displacements.

The MRI imaging sequence consisted of 1) a cross sectional image showing only the fluids in the fracture, Figure 2, and 2) a sagittal image to determine the saturation profile in both plugs and the fracture along the flow axis [7]. The dark circular band in the cross sectional image, Figure 2, is the Teflon® spacer while the slot at the top is an open section. This open section let the air out during assembly. The bright lines around the spacer are decane trapped between the spacer and the confining tubing.

Since the volume of rock needed for this study exceeded the amount of reservoir core available, an aging technique was used that reproducibly altered the wettability of selected outcrop chalk to the range that is representative of North Sea reservoirs [17-20]. One advantage of altering the wettability of this outcrop chalk over using reservoir core is that all of the altered chalk has the same pore geometry.

RESULTS AND DISCUSSION
Previously reported waterflood saturation developments are shown in Figure 3 and 4 to demonstrate the effect of wettability at a macroscopic scale, about 1 cm resolution, on wetting phase movement across fractures in large chalk blocks.

Figure 3 shows the time development of the 2-D brine saturation during the constant differential pressure, 40 mbar, waterflood of the strongly water-wet, fractured block CHP-4 with the fracture configuration shown in Figure 1b [21]. During the waterflood the brine saturation increased as a dispersed front through Block A, the inlet block. The water saturation in Block B was still at, or close to, S_{wi} while the matrix just across the fracture in Block A was approaching its final water saturation, S_{wf}. After Block A reached approximately its final water saturation and the fractures were filled with brine, the brine entered Block B. The general appearance of the saturation distribution in Block B suggested that the brine entered gradually from both the horizontal and vertical fractures between Blocks A and B. However, little, if any, water had crossed the fracture at 13 cm and entered into Block C at the time when 4th image was collected. When Block B approached its final water saturation, water moved into Block C, the outlet block. The slightly higher water saturation in the lowest part of the Block C, the outlet block, suggested gravity segregation in the open fracture.

Figure 4 shows the water saturation development during a typical waterflood in the fractured, moderately water-wet block, CHP-5 [2]. Most significantly, there was no detectable capillary hold up at the fractures; the water appeared to cross the closed fractures as if no fracture was present. The slightly lower saturation in the 5th image suggests that the open fracture affected the rate of movement of water into the outlet block C. Results from waterflooding several other blocks at moderately water-wet conditions corroborated these results [2-5,21-23].

High Resolution Wetting Phase Fracture Crossing. The NTI images of saturation development while waterflooding, Figures 3 & 4, dramatically show the macroscopic effect of fractures and wettability on the flow of fluids at fractures in fractured chalk. However, to determine the details of the oil recovery mechanisms in fractured reservoirs, fluid flow inside and across fractures at different wettability conditions was needed. Magnetic resonance imaging (MRI) provided the higher resolution, about 300 micrometers, needed to monitor the flow of fluids across fractures and into the matrix adjacent to the fracture. Figure 2 shows the fracture orientation used to experimentally simulate the fracture and a representative cross sectional MRI image of the fracture. This image shows the fracture filled with decane with a few dark spots, which were trapped air bubbles. Water, which appears later in the process, is also black. The dark ring around the outside of the image is the Teflon® spacer used to separate the plugs and the light area at the top is an open section in this spacer. The bright ring, at the outer edge of this image, is decane trapped between the Teflon® spacer and the containment sleeve. Images were also taken along the length of the two plugs, which show the decane saturation profiles in the two plugs and the fracture along the direction of flow.

Wettability: Figure 5 shows six time steps of the fluid saturation development in the 1 mm open fracture during the waterflood of a strongly water-wet stacked core system. Flow is from the inlet plug, behind the image plane, toward the reader and then out of the image plane, to enter the outlet plug. As can be seen from the figure, water breakthrough occurred at about 3450 min. and resulted in a rapid filling, approximately 150 min, of the fracture by the invading water. At the injection rate of 0.4 cc/hr, this corresponded to filling the fracture, ca. 1.1 cc, via a simple hydraulic mechanism. These observations corroborate the NTI experiments, Figure 3, which showed that at strongly water-wet conditions the inlet plug reached its spontaneous imbibition endpoint before water left the matrix and entered the fracture.

Figure 6 shows the development of fluid saturation in the 1 mm open fracture for eight time steps during the waterflood of the moderately water-wet, $I_w=0.7$, stacked core system. The sequence of images indicate that drops of water, the dark circles, formed on the exit face of the inlet plug and developed into bridges across the fracture, which grew in size with time. The water breakthrough across the fracture occurred quite early compared to the strongly water-wet waterflood, with the first water drops observed at about 2100 min. As the water bridges increased in size, gravity caused them to sag, coalesce, drop to the bottom and slowly fill the fracture. The fracture was completely filled with water before the imbibition endpoint in the first core was reached, about. 3100 min. The fracture filling process lasted for about 1000 min., compared to 150 min. at the strongly water-wet conditions. This indicated a dispersed water-front moving across the fracture, corroborating the macroscopic observations in the NTI block experiments at moderately water-wet conditions [3-5].

Figure 7 shows the development for the nearly neutral-wet plugs with a 2.3mm fracture. The sequence of images indicates that significantly larger drops of water, compared to the moderately water-wet plugs, formed. The water breakthrough was again quite early compared to the strongly water-wet waterflood. Some of the bridges crossed the fracture and grew in size with time. Consistent with the interpretation of how the bridges form, it

is evident that some of the bridges did not reach across this wider fracture, appearing as the lighter gray circles, and slowly slid towards the bottom of the fracture.

Fracture Width: Figures 8 and 9 show selective MRI images of the fracture crossing for fracture widths of 2.3 mm and 3.5 mm, respectively with moderately water-wet plugs, Iw=0.6. At 2.3 mm, Figure 8, a number of bridges formed and water was transported across the fracture well before the imbibition endpoint was reached. With a fracture of 3.5 mm a number of drops were observed early, gray colored circles, but few, if any, bridges formed. This indicated that a 3.5 mm fracture width was an effective barrier to the formation of bridges for these conditions. The saturation distributions along the flow axis showed that the 3.5 mm fracture stopped water flow until the fracture was hydraulically filled. The 2.3 mm fracture showed a more uniform water saturation across the fracture during the waterflood, similar to the 1 mm fracture. The significant end effect, for both widths, showed that capillary contact for decane was lost and decane was bypassed in the inlet plug.

Figures 10 and 11 show the fracture crossing between the nearly neutral-wet plugs for fracture widths of 2.3 mm and 3.5 mm, respectively. Bridges formed at both fracture widths, but the 2.3 mm fracture, Figure 10, formed drops before fracture filling began at the bottom while the 3.5 mm fracture, Figure 11, formed drops after filling began at the bottom. The formation of bridges in the 3.5 mm fracture substantiates the theory that at lower water wettability the drops are larger compared to the moderately water-wet chalk in Figure 9. The saturation distribution, as a function of time, along the flow axis was similar for both fracture widths. And, both fracture widths produced significant, but similar, end effects indicating that considerable decane was bypassed when the fracture was filled with water and decane continuity between the plugs was lost.

Injection Rate: Figure 12 shows a waterflood similar to that in Figure 5 but at a higher injection rate, to determine whether rate and accompanying pressure differential would change the fracture crossing mechanism. The results in Figures 12a, 12b, 12c show a) the water saturation profile along the flow axis as a function time b) the average saturation in the inlet and outlet core plugs and in the fracture as a function of time and c) a representative cross sectional MRI image of the fluid in the fracture during the waterflood. Figures 12a & 12b show that the inlet plug nearly reached its final water saturation before the water entered the fracture, about 4 hrs, and then after filling the fracture; entered the second plug. At the high flow rate used, the imbibition into the second plug was slower than the rate of the fracture filling. Figure 12c shows the water saturation in the 1 mm open fracture between the two halves of plug CPA-6.6 when the fracture was half-filled. No indications of water drops or bridges were observed. Even with the high spatial resolution in the images of ca. 300 micrometer little, if any, end effect, i.e. capillary hold up of the water, could be observed in the profiles parallel to the flow axis, Figure 12a. This experiment demonstrated that no fracture crossing by water bridges occurred at strongly water-wet conditions, even at a flow rate 5 times the field-relevant flow rate.

At the higher injection rate, 2.0 cc/hr, the moderately water-wet plugs performed quite similarly to the same plugs at the lower rate of injection. When the fracture began filling

from the bottom drops, gray circles, were observed in the fracture, Figure 13, but they did not form bridges across the fracture. At the higher rate the end effect was measurably greater compared to slower rate of water injection. The most notable observation was the formation of decane bridges after the fracture was water filled, which allowed the bypassed decane access to the outlet plug. These results indicate that a 3.5 mm fracture would prevent the establishment of viscous forces across the fracture.

For the nearly neutral-wet plugs the higher rate of injection caused the fracture to fill only from the bottom, Figure 14. There apparently was not enough time for the drops to form as was observed during the slower injection rate. The saturation profiles along the flow axis showed a significantly greater end effect than was observed at the slower rate. This bypassed decane, even after 1 pore volume of injected water, was almost at its original saturation near the fracture. Decane formed drops and bridges even before the fracture was completely filled with water.

Discussion of MRI Monitoring Waterflooding the Stacked Core Systems. The MRI images of oil saturation development in the fracture clearly revealed two distinct transport mechanisms for the wetting phase across the fracture depending on the wettability, schematically illustrated in Figure 15. When the plug was strongly water-wet, oil production was dominated by capillary forces, which caused the inlet plug to reach its spontaneous imbibition endpoint before water could leave the matrix and enter the fracture. The fracture crossing mechanism was a hydraulic displacement of oil upward at the rate of water injection. At less-water-wet conditions, water drops formed on the exit face of the inlet plug and grew large enough to form bridges across the open space between the two plugs. This happened, well before the inlet plug reached its spontaneous imbibition endpoint. Thus, both the wetting and non-wetting phases maintained contact across the fracture. Under these conditions, the fracture filled slowly, as the bridges increased in diameter and additional bridges formed. Due to the capillary continuity provided by the wetting phase bridges, a viscous pressure drop was established across the stacked core plugs, producing a viscous component to the total oil recovery. The number of bridges appeared to be dependent on the fracture width, the matrix wettability and the rate of flow. This implies an interplay between the viscous pressure, controlling the bubble growth, and the interfacial tension between the water and the decane. The wettability at the exit face controls the contact angle of the drops, thus the maximum drop size at the given pressure differential and interfacial tension, and therefore determines the ability of the wetting phase fracture crossing.

CONCLUSIONS

- Fractures significantly affected water movement during water flooding at strongly water-wet conditions, but not at moderately water-wet conditions.
- The MRI images of oil saturation development in the fracture revealed two distinct transport mechanisms for the wetting phase to cross a fracture at different wettability conditions.
- At strongly water-wet conditions, $I_w=1.0$, water did not enter an open fracture before the spontaneous imbibition endpoint was reached, even at flow rates 5

times the field relevant flow rate. Water then filled the fracture by hydraulic displacement of the decane.

- At moderately water-wet conditions, $I_w=0.6$, wetting phase bridges were formed before the spontaneous imbibition endpoint was reached, causing water to readily flow across an open fractures before Pc became zero at the inlet plug's outlet face.
- At nearly neutral-wet conditions, $I_w=0.3$, wetting phase bridges appeared to form earlier allowing the water to readily cross the 1 mm and 2.3 mm open fractures.
- The width that the bridges could cross was dependent on the rate of water injection, with more bridges at the higher rate.
- The possibility of forming bridges is dependent on fracture width with bridges more likely to form at smaller widths and not forming beyond a critical width.

ACKNOWLEDGEMENT

REFERENCES

1. Baldwin, B. A., King, R.: "Why Would an Oil Company use MRI", Spatially Resolved Magnetic Resonance (Methods, materials, Medicine, Biology, Rheology, Geology, Ecology, Hard Wave) Eds. P. Blumler, B. Blumich, R. Botto and E. Fukushima (Wiley-VCH, New York, 1999).
2. Graue, A., Viksund, B.G., Baldwin, B.A., Spinler, E.: "Large Scale Imaging of Impacts of Wettability on Oil Recovery in Fractured Chalk", SPE Journal, Vol 4, No. 1, (25-36), March 1999.
3. Graue, A., Bognø, T., Baldwin, B.A., Spinler, E.A.: "Wettability Effects on Oil Recovery Mechanisms in Fractured Reservoirs", SPE74335, SPEREE, Vol. 4 , No. 6 , (455-466), Dec. 2001.
4. Graue, A., Moe, R.W., Baldwin, B.A.: "Comparison of Numerical Simulations and Laboratory Waterfloods with *In-Situ* Saturation Imaging of Fractured Blocks of Reservoir Rocks at Different Wettabilities", SPE59039, 2000 SPE Internatl. Petr. Conf. And Exh., Villahermosa, Mexico, Febr. 1-3, 2000.
5. Graue, A., Moe, R.W., Bognø, T.: "Impacts of Wettability on Oil Recovery in Fractured Carbonate Reservoirs", Reviewed Proc.: 2000 International Symposium of the Society of Core Analysts, Abu Dhabi, United Arab Emirates, Oct. 18-22, 2000.
6. Graue, A., Aspenes, E., Moe, R.W., Baldwin, B.A., Moradi, A., Stevens, J., Tobola, D.P.: "MRI Tomography of Saturation Development in Fractures During Waterfloods at Various Wettability Conditions", SPE 71506, Proc: 2001 SPEATCE, New Orleans, Louisiana, 30 Sept.- 3 Oct., 2001.
7. Aspenes, E., Graue, A., Baldwin, B.A., Moradi, A., Stevens, J.,Tobola, D.P.: "Fluid Flow in Fractures Visualized by MRI During Waterfloods at Various Wettability Conditions – Emphasis on Fracture Width and Flow Rate", SPE 77338, Proc.: SPE Annual Technical Conference and Exhibition, San Antonio, Texas, 29 September–2 October 2002.
8. Horle, T., Firoozabadi, A., and Ishimoto, K., "Laboratory Studies of Capillary Interaction in Fracture/Matrix Systems" SPERE, (353-60), 1990.
9. Amott. E.: "Observations Relating to the Wettability of Porous Rock", Trans., AIME 1959 216, 156-162.

10. Bailey, N.A., Rowland, P.R., Robinson, D.P.: "Nuclear Measurements of Fluid Saturation in EOR Flood Experiments", Proc.: 1981 European Symposium on Enhanced Oil Recovery, Bornmouth, England, Sept. 21-23, 1981.

11. Lien, J.R., Graue, A. and Kolltveit, K.: "A Nuclear Imaging Technique for Studying Multiphase Flow in a Porous Medium at Oil Reservoir Conditions", Nucl. Instr. & Meth., A271, (693-700), 1988.

12. Graue, A., Kolltveit, K., Lien, J.R. and Skauge, A.: "Imaging Fluid Saturation Development in Long Coreflood Displacements", SPEFE, Vol.5, No.4, (406-412), (Dec., 1990).

13. Graue, A.: "Imaging the Effect of Capillary Heterogeneites on Local Saturation Development in Long-Core Floods", SPEDC, Vol. 9, No. 1, (57-64), March 1994.

14. Rothwell, W.P., "Nuclear Magnetic Resonance Imaging", App. Opt. Vol. 24, (pp 3958), 1985.

15. Mandava, S.S., Watson, A.T. and Edwards, C.M., "NMR Imaging of Saturation during Immiscible Displacements", AIChE J. Vol. 36, (1680-6), 1990.

16. B.A. Baldwin and E.A. Spinler: "In Situ Saturation Development during Spontaneous Imbibition", J. Petroleum Sci. & Engr. (230-32), 2002.

17. Aspenes. E., Graue, A., Ramsdal, J.: "In-Situ Wettability Distribution and Wetting Stability in Outcrop Chalk Aged in Crude Oil", Proc.: 7th International Symposium on Reservoir Wettability and Improved Oil Recovery, Tasmania, Australia, March 12-15, 2002.

18. Graue, A., Tonheim, E. and Baldwin, B.: "Control and Alteration of Wettability in Low-Permeability Chalk", Proc.: 3rd International Symposium on Evaluation of Reservoir Wettability and Its Effect on Oil Recovery, (123-128), Laramie, WY., USA, Sept., 1995.

19. Graue, A., Viksund, B.G., Baldwin, B.A: "Reproducible Wettability Alteration of Low-Permeable Outcrop Chalk", SPE Res. Eng. and Eval., Vol. 2, No. 2, (134-140), April 1999.

20. Graue, A., Aspenes, E. Bognø, T., Moe, R.W., and Ramsdal, J.: "Alteration of Wettability and Wettability Heterogeneity", J. Petr. Sci. & Eng. 33, (3-17), 2002.

21. Viksund, B.G., Eilertsen T., Graue, A., Baldwin, B. and Spinler, E.: "2D-Imaging of the Effects from Fractures on Oil Recovery in Larger Blocks of Chalk", Reviewed Proc.: International Symposium of the Society of Core Analysts, Calgary, Canada. (Sept. 8-10, 1997).

22. Viksund, B.G., Graue, A., Baldwin, B. And Spinler, E.: "2-D Imaging of waterflooding a Fractured Block of Outcrop Chalk". Proc.: 5th Chalk Research Symposium, Reims, France, (Oct. 7-9, 1996).

23. Graue, A., Nesse, K.: "Impact of Fracture Permeability on Oil Recovery in Moderately Water-Wet Fractured Chalk Reservoirs", Proc.: SPE/DOE Thirteenth Symposium on Improved Oil Recovery, Tulsa, Oklahoma, 13–17 April 2002.

Table 1. Fluid Properties				
Fluid	Density [g/cm^3]	Viscosity [cP] at 20°C	Viscosity [cP] at 90°C	Composition
Brine	1,05	1,09		5 wt% NaCl + 3.8 wt% CaCl$_2$
n-Decane	0,73	0,92		
Decahydronaphtalene	0,896			
Crude oil	0,849	14,3	2,7	

Table 2. Experimental Data for Chalk Blocks

Block	CHP-4		CHP-5	
Outcrop	Portland		Portland	
Location	Ålborg		Ålborg	
Length (cm)	20		20	
Height (cm)	13		12	
Thickness (cm)	5,5		5,5	
Abs. Permeability (mD)	1,8		3	
Porosity (%)	45		45	
Pore Volume (ml)	648		585	
MISC. FLOOD # :	1		1	
Flow Rate (ml/hr)	25		20	
OILFLOOD # :	1	2	1	
Oil Viscosity (cP)	0,92	0,92	0,92	
S_{wi} (%PV)	100	65	100	
dS_w (%PV)	73	39	73	
S_{wf} (%PV)	27	26	27	
Max Pressure (Bar)			28	
Endpoint Eff. Perm. to oil (mD)	2	1,6[a]/4,6[b]	/3	
AGING :	NO		YES	
Aging Temp. (deg. C)			90	
Aging Time (days)			2.5	
Amott index after aging			0.8	
Oil flooding prior to imb. :				
Decaline (PV)			5	
n-Decane (PV)			5	
Endpoint eff. Perm. to oil (mD)				
WATERFLOOD # :	1	2	1	2
Block Condition	Whole	Fractured	Whole	Fractured
Cutting		Hand Saw		Band Saw
Oil Viscosity (cP)	0,92	0,92	0,92	0,92
S_{wi} (%PV)	27	26	27	26
dS_w (%PV)	38	40	42	41
S_{wf} (%PV)	65	66	69	67
Endpoint Eff. Perm. to water (mD)	0,4	,6	0.9	2.2
Oil Recovery (%OIP)	52	54	58	56
Flow Rate (ml/hr)			1	1

[a] Whole block

[b] Fractured block, embedded fracture network

[c] Fractured block, interconnected fracture network

Table 3. Core Properties

Core	Length [cm]	Diameter [cm]	Porosity [%]	Abs. Perm [mD]	Iw
6,1	6,02	3,82	46,8	4,0	0.6
6,4	6,04	3,82	46,8	3,8	0.3
6,6	6,02	3,81	44,3	4,6	1.0
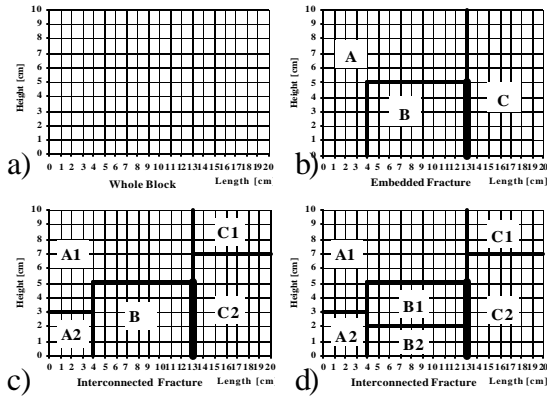
Figure 1. The fracture networks used in the block experiments.
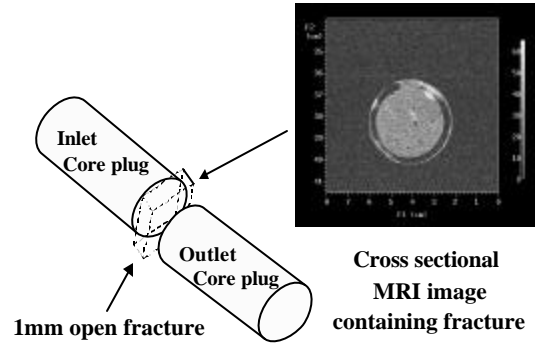
Figure 2: Cross sectional image.
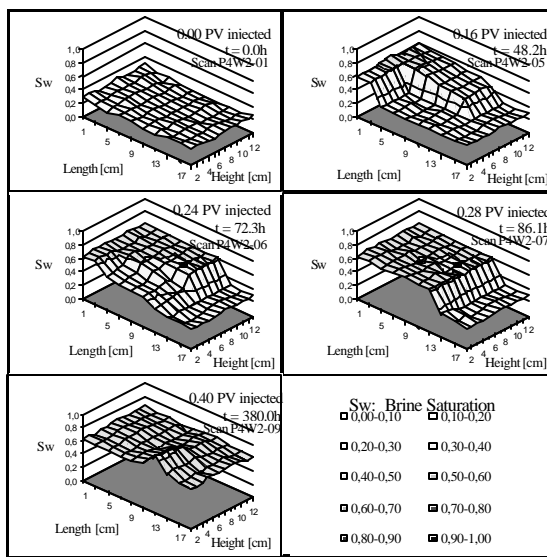
Figure 3. Water saturation development while waterflooding the fractured strongly water-wet block CHP-4.
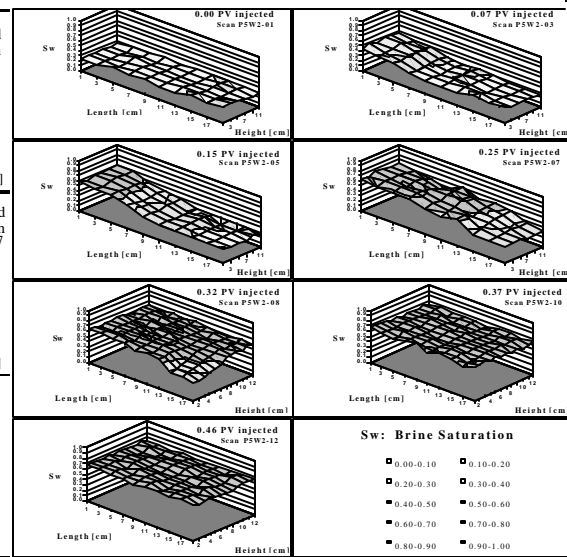
Figure 4. Water saturation development while waterflooding the fractured moderately water-wet block CHP-5.
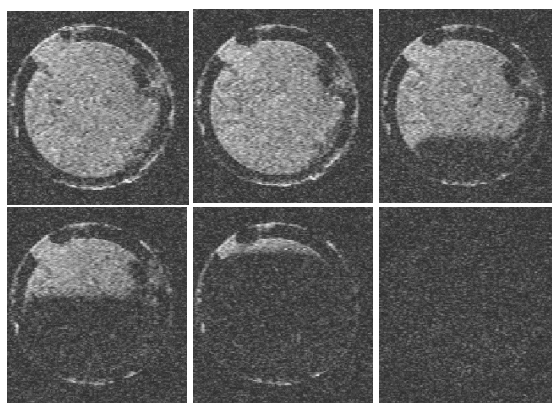

Figure 5. Cross sectional MRI image of the oil saturation in the 1mm fracture during the wet core plugs.
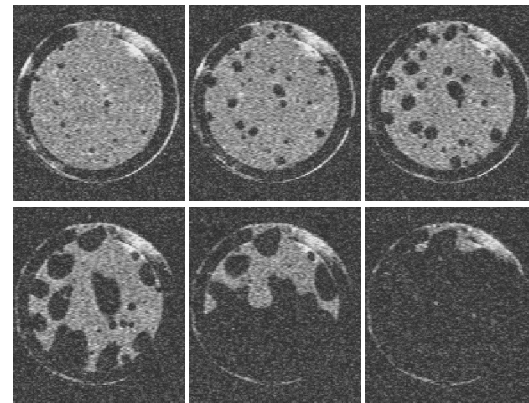

Figure 6. Cross sectional MRI image of the oil saturation in the 1mm fracture during the waterflood of the stacked moderately water-wet core plugs at $I_w = 0.7$.
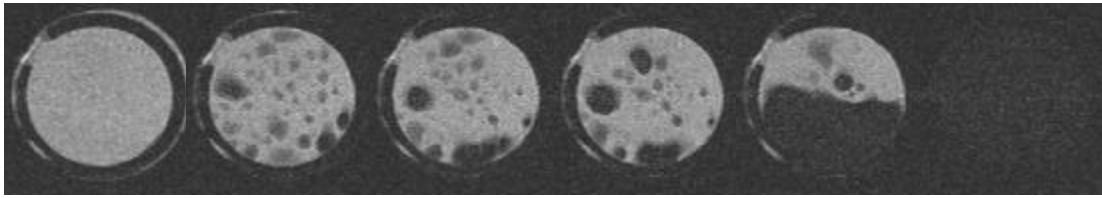
Figure 7. Cross sectional MRI image of the oil saturation in the 2.3mm fracture during the waterflood of the nearly neutral-wet stacked core plugs at $I_w = 0.3$.
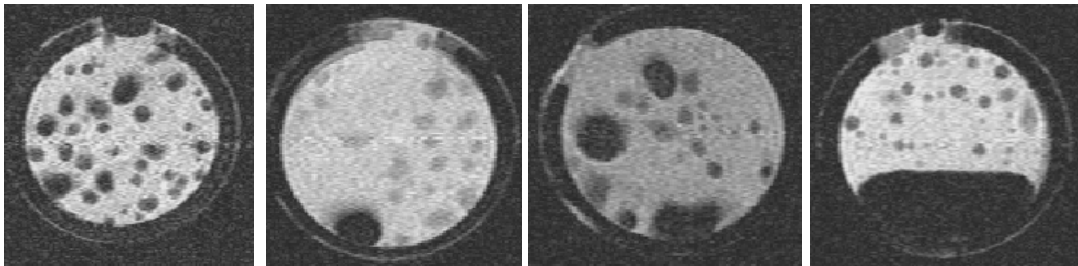
Figure 8. MRI cross-section of fracture; I_w=0.6, Flow rate=0.4cc/hr, Width=2.3mm

Figure 9. MRI cross-section of fracture; I_w=0.6, Flow rate=0.4cc/hr, Width=3.5mm

Figure 10. MRI cross-section of fracture; I_w=0.3, Flow rate=0.4cc/hr, Width=2.3mm

Figure 11. MRI cross-section of fracture; I_w=0.3, Flow rate=0.4cc/hr, Width=3.5mm
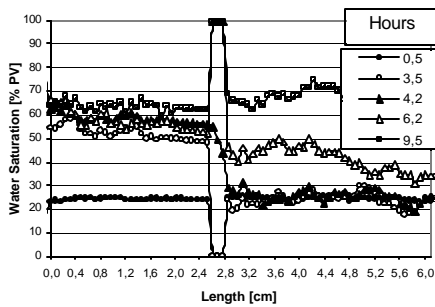
Figure 12a. 1D-Brine saturation profiles; I_w=1.0, Flow rate=2.0cc/hr, Width= 1.1mm
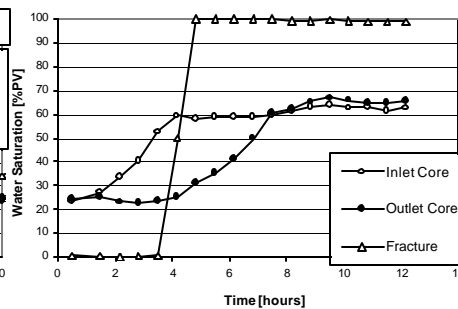
Figure 12b. Brine saturation development; I_w=1.0, Flow rate=2.0cc/hr, Width= 1.1mm
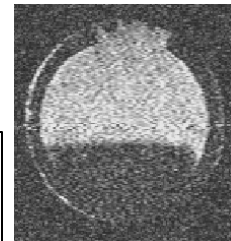
Figure 12c. MRI cross-section of fracture,; I_w=1.0, Flow rate=2.0cc/hr, Width= 1.1mm
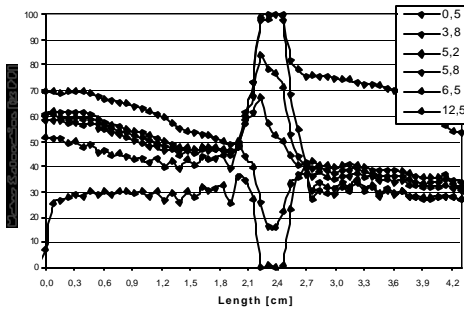
Figure 13a. 1D-Brine saturation profiles; I_w=0.6, Flow rate=2.0cc/hr, Width= 3.5mm
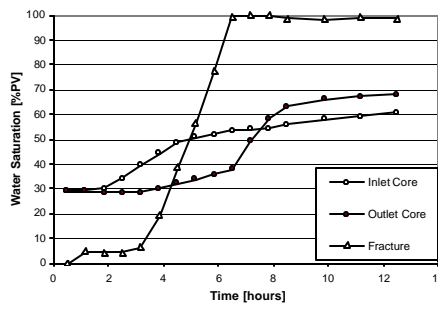
Figure 13b. Brine saturation development; I_w=0.6, Flow rate=2.0cc/hr, Width= 3.5mm
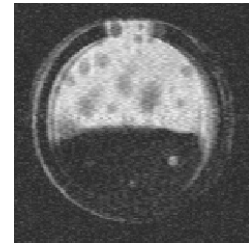
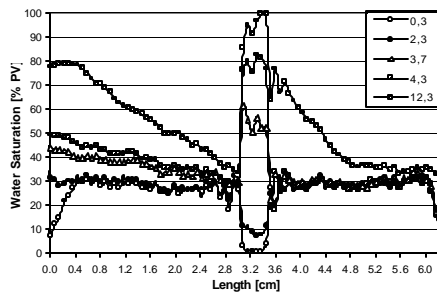**Figure 13c. MRI cross-section of fracture, I_w=0.6, Flow rate=2.0cc/hr, Width= 3.5mm**

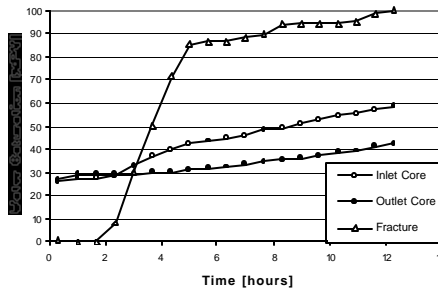**Figure 14a. 1D-Brine saturation profiles; I_w=0.3, Flow rate=2.0cc/hr, Width= 3.5mm**

Figure 14b. Brine saturation development I_w=0.3, Flow rate=2.0cc/hr, Width= 3.5mm
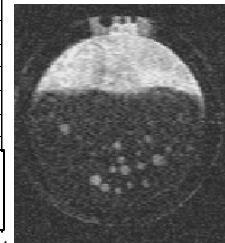
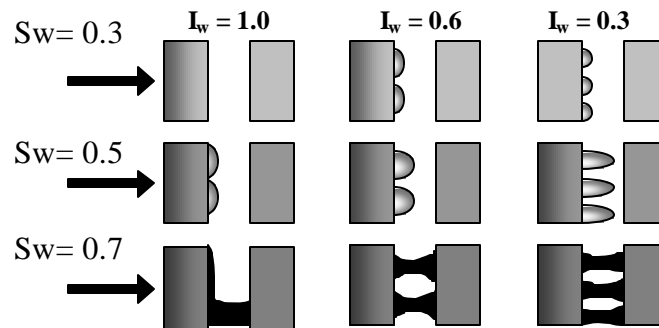**Figure 14c. MRI cross-section of fracture, I_w=0.3, Flow rate=2.0cc/hr, Width= 3.5mm.**

Fig. 15. Schematics of wetting phase fracture crossing.